Author/s:
Wibowo, SH;Sulistio, A;Wong, EHH;Blencowe, A;Qiao, GG

Title:
Functional and Well-Defined β-Sheet-Assembled Porous Spherical Shells by Surface-Guided Peptide Formation

Date:
2015-06-01

Citation:
Wibowo, S. H., Sulistio, A., Wong, E. H. H., Blencowe, A. & Qiao, G. G. (2015). Functional and Well-Defined β-Sheet-Assembled Porous Spherical Shells by Surface-Guided Peptide Formation. Advanced Functional Materials, 25 (21), pp.3147-3156. https://doi.org/10.1002/adfm.201404091.

Persistent Link:
https://hdl.handle.net/11343/54981

DOI: 10.1002/ ((please add manuscript number))
Article type: Full Paper

Functional and Well-defined *β*-sheet-assembled Porous Spherical Shells by Surface-guided Peptide Formation

*Steven Harris Wibowo, Adrian Sulistio, Edgar H. H. Wong, Anton Blencowe and Greg G. Qiao**

S. H. Wibowo, Dr. Adrian Sulitio, Dr. Edgar H. H. Wong and Prof. G. G. Qiao
Dept. Chemical and Biomolecular Engineering
The University of Melbourne,
Parkville, VIC 3010, Australia
E-mail: gregghq@unimelb.edu.au

Dr. A. Blencowe
Division of Information Technology, Engineering and the Environment
University of South Australia
Mawson Lakes, SA 5095, Australia

Keywords: *β*-sheets, ring-opening polymerization, surface grafting, thin shells, polypeptide

Abstract

Polypeptides have attracted widespread attention as building blocks for complex materials due to their ability to form higher-ordered structures such as β-sheets. However, the ability to precisely control the formation of well-defined β-sheet-assembled materials remains challenging as β-sheet formation tends to lead to ill-defined and unprocessable aggregates. This work reports a simple, rapid and robust strategy to form well-defined peptide β-sheet-assembled shells (i.e., hollow spheres) by employing surface-initiated *N*-carboxyanhydride ring-opening polymerization under a highly-efficient surface-driven approach. The concept is demonstrated by the preparation of enzyme-degradable rigid shell architectures composed of H-bonded poly(L-valine) (PVal) grafts with porous and sponge-like surface morphology. The porous PVal-shells exhibit a remarkable and unprecedented ability to non-covalently entrap metal nanoparticles, proteins, drug molecules and bio-relevant polymers, which could potentially lead to a diverse range of biodegradable and functional platforms for applications ranging from therapeutic delivery to organic catalysis.

1. Introduction

Proteins and polypeptides have received widespread scientific interest as renewable building blocks for the assembly of nanomaterials with tailored structural and chemical functions that are not easily accessible using traditional organic molecules and polymers.[1, 2] Amongst the fascinating properties of polypeptides (i.e., sequence specific function, biocompatibility and degradability), their ability to form hierarchically ordered structures, including α-helices and β-sheets, has been intensively studied with particular emphasis on understanding the structure-activity relationships important to nearly all biological processes and the engineering of natural biomaterials.[3, 4] For instance, the inclusion of β-sheet secondary structures has been identified as an important component that endows spider and silkworm silks with superior mechanical strength.[5] Inspired to understand and mimic these

natural phenomena, much research has been directed towards employing *β*-sheet forming peptides as a non-covalent stabilization force to form stable and complex architectures.[6, 7-9] However, since *β*-sheet forming polypeptides are typically hydrophobic and non-ionic, the synthesis of well-defined architectures from such peptides has been challenging as they tend to aggregate uncontrollably and form insoluble, ill-defined structures.[10, 11] To avoid such issues, conventional approaches involve the self-assembly of amphiphilic block copolymers composed of (sequence-controlled) short *β*-sheet forming motifs and long hydrophilic polymer/polypeptide blocks to form tubular architectures.[7, 9, 12, 13] For example, Stupp and co-workers reported the formation of nanofibres from self-assembled peptide amphiphiles composed of a hydrophobic alkyl-tail, a structural peptide sequence with a high propensity for *β*-sheet formation, and a terminal hydrophilic peptide sequence containing charged (bioactive) residues.[12, 14] These self-assembled nanofibres have been successfully applied to bone re-growth and nerve recovery.[15] A different approach pioneered by Ghadiri et al. employed cyclic peptide structures made up of alternating D- and L-amino acid residues as building block.[16, 17] These peptide subunits can then self-assemble (i.e., 'stack') to form H-bonded peptide nanotubes with *β*-sheet-like secondary structures. Although these approaches have furnished well-defined *β*-sheet-stabilized architectures, they require multi-step synthesis of sequence-specific amphiphilic/cyclic precursors using specialized instruments (e.g., automated peptide synthesisers) and precisely-balanced hydrophobic/hydrophilic segments, as well as meticulously-controlled self-assembly conditions. Furthermore, the architectures obtained from these self-assembly approaches are mostly limited to tubular-shapes. It is important to have the ability to form other well-defined shapes of *β*-sheet-stabilised peptide architectures for application in various other unexplored fields.[18] Ring-opening polymerization (ROP) of *α*-amino acid *N*-carboxyanhydrides is an effective method to form polypeptide with high molecular weights and low polydispersity. However, insoluble *β*-sheet aggregates are formed when *β*-sheet forming *α*-amino acid *N*-carboxyanhydrides are

polymerized in solution via ROP. Therefore, it is necessary to control the formation of *β*-sheet architectures in a confined space. It is the aim of this study to develop a synthetic approach for the facile preparation of novel peptide architectures to overcome the abovementioned challenges.

We hypothesised that a new approach to fabricate novel well-defined architectures composed solely of *β*-sheet forming peptides would be to use a surface-confined bottom-up strategy employing *α*-amino acid derivatives as building blocks. Specifically, by taking advantage of surface-initiated ring-opening polymerization (SI-ROP) of (*β*-sheet forming) *α*-amino acid *N*-carboxyanhydrides to form grafted polypeptides, we herein report a simple, rapid and robust strategy to form novel polypeptide *β*-sheet architectures with tailored shapes and dimensions (**Scheme 1**). As the polypeptides remain anchored onto the template surface, the formation of *β*-sheet-forming peptide grafts is controlled in a spatial and temporal fashion, avoiding the unconstrained random aggregation of polypeptides formed in solution. Our study reveals that after a certain SI-ROP time, H-bonding between the surface-anchored peptide grafts results in *β*-sheet architectures assembled *in situ* that possess a rigid and porous structured surface. Since both the polypeptide formation and self-assembly into *β*-sheet structures are surface-driven, the resulting H-bonded peptide grafts adopt the three-dimensional (3D) shape of the template. Following template dissolution, stable and well-defined free-standing polypeptide shell architectures were formed. Given the versatility of this synthetic approach and the availability of a broad range of potential templates with different shapes and sizes, this strategy enables the fabrication of various shell sizes and shapes currently not accessible by any existing methods.

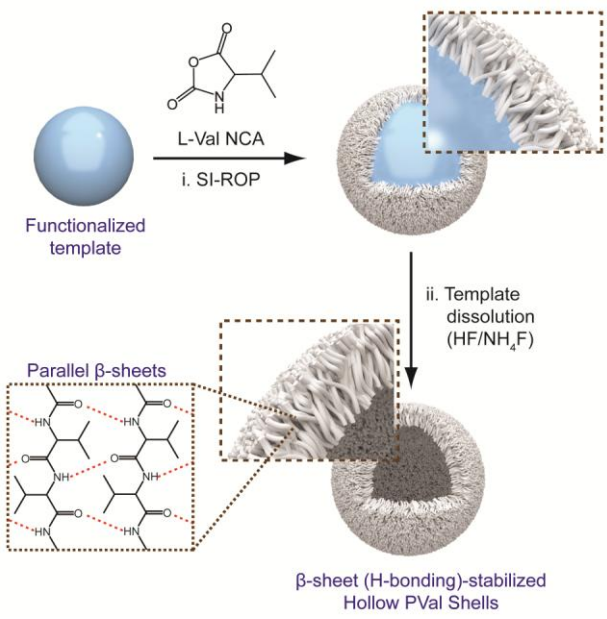

Scheme 1. Surface-guided formation of peptide *β*-sheet architectures via i) surface-initiated ROP of L-valine NCA from aminated silica particles, and ii) subsequent template dissolution, resulting in the formation of *β*-sheet-stabilized hollow poly(L-valine)-shells.

2. Results and Discussion

To demonstrate the general principal of this new surface-driven approach, non-porous spherical silica particles (5.0 ± 0.2 μm diameter) were selected as templates and were initially subjected to silanization with 3-aminopropyl triethoxysilane (APTS).[19] The amine-functionalized particles were then employed in the SI-ROP of L-valine NCA (Val-NCA) to generate films composed of grafted poly(L-valine) (PVal) chains. L-Valine is a cheap, naturally-occurring and essential amino acid found in all living organisms, and has been approved by U.S. Food and Drug Administration as a direct food additive. Furthermore, the NCA derivative of L-Valine is an excellent model monomer as the resulting polypeptide (i.e., PVal) preferentially adopts *β*-sheet conformations.[20] As a result of the high propensity of PVal to form *β*-sheets, it is hypothesized that as the PVal chains grow from the silica template, intermolecular H-bonding between the PVal backbones results in the formation of *β*-sheets, thereby interlocking the grafts in place. The *in situ* generated *β*-sheet secondary structures provide a strong non-covalent stabilization mechanism that allows for the film

structure to remain intact upon subsequent dissolution of the silica template, yielding free-standing β-sheet-assembled PVal films in the form of hollow spherical shells (**Scheme 1**).

2.1. SI-ROP and *in situ* Formation of β-sheet

We first investigated the influence of polymerization time on the formation of PVal grafts and β-sheet secondary structures by terminating SI-ROP after predetermined reaction times (15 min to 24 h). The isolated PVal-coated silica particles were then analyzed via Fourier transform infrared (FT-IR) spectroscopy (**Figure 1A**). FT-IR spectroscopic analysis of the bare silica particles revealed characteristic peaks (Supplementary Information (SI), **Figure S1**), including intense and broad bands at 1040 and 1093 cm^{-1} assigned to the Si-O-Si asymmetric stretching vibrations,[22] which can also be clearly observed in the FT-IR spectra of the PVal-coated silica particles isolated at various polymerization times (**Figure 1A** and SI, **Figure S1**). Amongst the infrared active amide vibrations of polypeptides/proteins, the Amide I band (C=O stretch; peptide backbone) typically exhibits the most prominent peak between 1600 and 1700 cm^{-1}.[23, 24] In this study, the Amide I band appears at 1640 cm^{-1} within 15 min of SI-ROP, indicating the presence of PVal grafts on the silica template (**Figure 1A**). Notably, with longer polymerization times the intensity of this Amide I band increases and shifts slightly to 1637 cm^{-1} (**Figure 1A** and SI, **Figure S1**; band values are provided in SI, **Table S1**). Peak deconvolutions using a Lorentzian fit were then performed on the Amide I band and the asymmetric Si-O-Si vibrations (at 1040 and 1093 cm^{-1}) to investigate the increase in Amide I intensity relative to the silica template. The ratio of these peak areas increases from 0.02 to 0.79 after 15 min and 24 h of SI-ROP, respectively (**Figure 1B** and **Table S1** (SI)), which strongly suggests the presence of longer PVal grafts at longer polymerization times. The increase in peak intensity was also observed for other amide vibrations associated with the PVal backbone and side-chain (**Figure 1A** and SI, **Figure S1**). Whereas the Amide A and B bands (N-H stretching vibrations) appeared at *ca.* 3280 and 3082 cm^{-1}, respectively, the

Amide II (in-plane N-H bending and C-N stretch) and V (N-H out-of-plane bending) bands were observed at 1547 and 714 cm^{-1}, respectively. Furthermore, the FT-IR spectra also display PVal aliphatic side-chain peaks at 2965, 1467 and 1397 cm^{-1} corresponding to C-H stretch, C-H bend and C-H methyl rock, respectively.

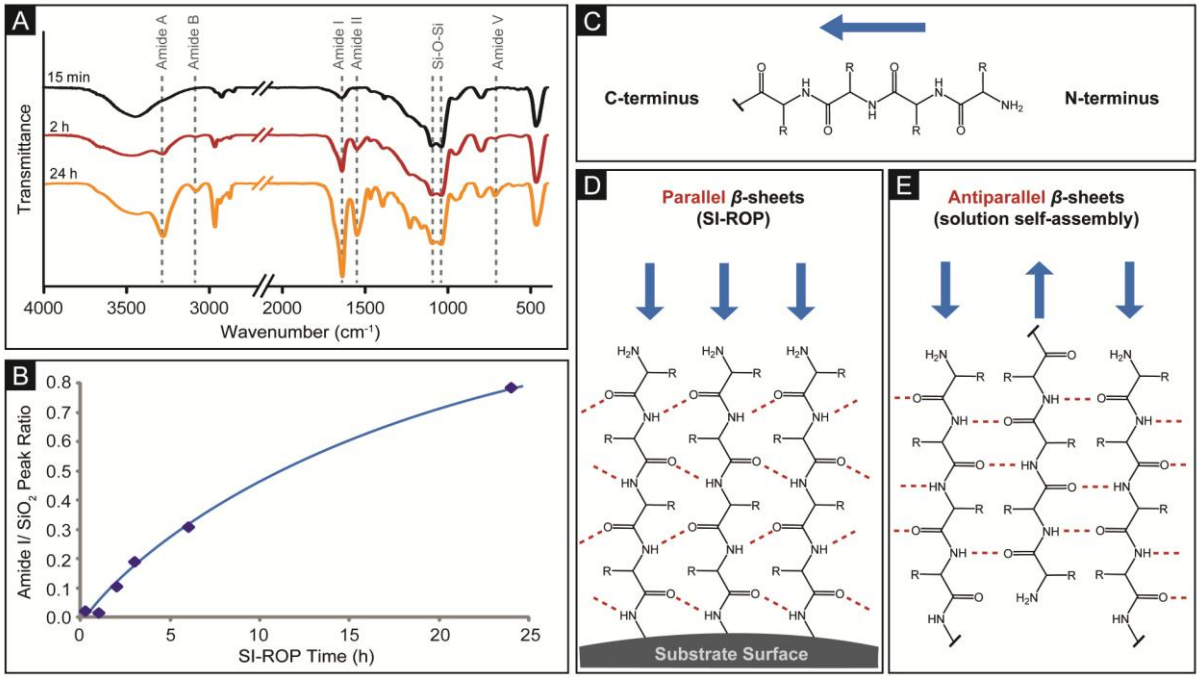

Figure 1. A) FT-IR spectra of PVal-coated silica templates after 15 min, 2 h and 24 h of SI-ROP. B) Ratio between Amide I/ SiO2 IR peaks with SI-ROP time. C) General structure of a polypeptide with a representative arrow pointing towards from the *N*-terminus to *C*-terminus of a polypeptide chain. D) H-bonding pattern of parallel *β*-sheets promoted by SI-ROP and E) H-bonding pattern of antiparallel *β*-sheets.

The secondary structure of the PVal-coated silica templates was also identified using FT-IR. The Amide I band (C=O stretch vibration) is the most sensitive spectral region towards polypeptide secondary structure and thus, the location of the Amide I peak has been widely used to determine peptide conformation.[9, 23-25] Previous studies have shown that the Amide I band occurs between 1650-1655 cm^{-1} for *α*-helical peptides.[25] Meanwhile, *β*-sheet structured peptides can be further categorized into parallel and anti-parallel, depending upon

the spatial organization of the polypeptide chains (**Figure 1C-E**).[26] Anti-parallel *β*-sheets exhibit a strong Amide I band between *ca.* 1620 - 1632 cm^{-1} and a second band at *ca.* 1680 - 1690 cm^{-1}.[25, 27] On the other hand, the Amide I band for parallel *β*-sheets occurs between *ca.* 1636 - 1640 cm^{-1}.[9] In addition, the distinction between peptide secondary structures can be made by the location of the Amide V band, whereby bands between *ca.* 610 - 620 cm^{-1} are assigned to *α*-helices and bands at *ca.* 700 cm^{-1} correspond to *β*-sheets.[24, 26, 28] In the FT-IR spectra obtained (**Figure 1A**), both the Amide I and Amide V bands strongly indicate that the PVal grafts adopt parallel *β*-sheet conformations (SI, **Table S1**). This conformation agrees with previous studies which demonstrated that valine residues have 'conformational preference' to form *β*-sheets.[20, 29] Also, as a result of the surface-initiated synthetic strategy, the C-termini of the PVal grafts are tethered to the silica surface during SI-ROP, which forces the C- and N- termini of the PVal grafts to be aligned in the same direction and thus promotes the formation of parallel *β*-sheets (**Figure 1D**). In nature, parallel β-sheets are less frequently found (accounting for only 14.9 % of *β*-sheet structures) as a result of the intrinsically favoured formation of anti-parallel or mixed *β*-sheets.[29] To the best of our knowledge, fabrication of well-defined peptide architectures assembled from parallel *β*-sheets is yet to be reported. In fact, studies involving the self-assembly of peptide/polymer amphiphiles in solution typically results in the formation of anti-parallel or mixed *β*-sheets.[13, 26] To confirm this, we also carried out a control experiment by conducting ROP of Val-NCA in solution, using *α*-methoxy, *ω*-amino heterofunctional poly(ethylene glycol) as a macroinitiator. As expected, subsequent FT-IR analysis of the resulting amphiphiles revealed Amide I bands at 1634 and 1679 cm^{-1}, confirming the anti-parallel/mix *β*-sheet conformation (**Figure S2**). Notably, this control experiment demonstrates that our surface- driven approach promotes the formation of solely parallel *β*-sheets that are rarely found and not easily achieved by self-assembly in solution.

2.2. Formation of *β*-sheet-assembled Porous Spherical Shells

To further investigate the role of H-bonding (i.e., *β*-sheet formation) as a stabilization force, we dissolved the underlying silica template after terminating SI-ROP at predetermined times (15 min to 24 h). Differential interference contrast (DIC) micrographs of the isolated structures reveal that for short polymerization times (< 1 h), only fragments or deformed PVal films were observed (**Figure 2A**). This is not surprising as the limited H-bonding between short PVal grafts may not provide sufficient mechanical stability to form free-standing architecture following dissolution of the template. However, with longer polymerization times (> 1 h), the increased intermolecular H-bonding between longer PVal grafts resulted in the formation of stable hollow architectures we refer as PVal-shells (**Figure 2A**) because of their rigid and hard surface coating. The free-standing hollow shells exhibit porous sponge-like structures readily visible in scanning electron microscopy (SEM) and transmission electron microscopy (TEM) images (**Figure 2B-C**). The observed porous morphology is believed to result from 'bundling' of the PVal-grafts as they H-bond and adopt crystalline *β*-sheet regions. The bundling of the PVal-grafts leads to the formation of a network-like structure, which not only provides mechanical stability but also results in the porous morphology. FT-IR analysis of the PVal-shells (**Figure 2D**) revealed the absence of bands associated with silica particles (e.g., Si-O-Si stretches at 1040 and 1093 cm^{-1}), confirming the complete removal of the silica template. Furthermore, the Amide I band at 1637 cm^{-1} and Amide V band at 712 cm^{-1} were clearly observed, which demonstrates that upon template removal, the H-bonded PVal grafts retain their parallel *β*-sheet conformations.[23-25] This secondary structure was further corroborated by x-ray diffraction, which revealed prominent peaks characteristic of *β*-sheets at 8° and 19°, corresponding to *d* spacings of 1.1 and 0.4 nm, respectively (**Figure 2E**).[13, 26, 30] This secondary structure is consistent with the proposed mechanism, whereby film stabilization is induced by the formation of *β*-sheets.

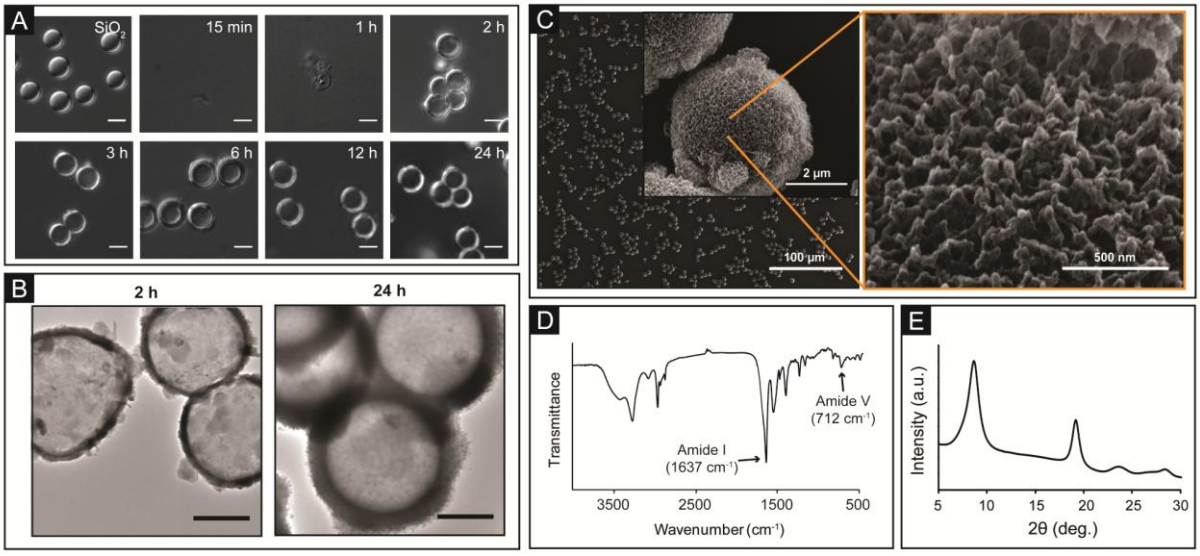

Figure 2. A) Evolution of PVal free-standing architectures with SI-ROP time as characterised by DIC microscopy (scale bars are 5 µm). B) TEM images of hollow shell architectures after 2 h and 24 h SI-ROP. C) SEM images of PVal-shells at various magnification (scale bars are 100 µm, 2 µm, and 500 nm with increasing magnification). D) FT-IR spectrum and E) XRD profile of PVal-shells revealing distinctive peaks corresponding to the parallel *β*-sheets.

The change in the PVal-shells' wall thickness after 2 and 24 h of polymerization was determined using TEM images of air-dried shells (**Figure 2B**), which revealed slight shrinkage of the shells with inner diameters of 4.0 ± 0.2 µm. Shrinkage during drying is a commonly observed phenomenon for capsules or vesicles.[31] Estimation of the PVal-shells' wall thicknesses by TEM (n > 15 for each time point) provided single-wall thicknesses of 200 ± 38 nm and 580 ± 48 nm for shells isolated after 2 and 24 h of polymerization, respectively. The shrinkage of shells upon drying was also observed during SEM analysis, which also corroborates the estimated wall thickness (**Figure S3**). This study demonstrates that the shell thickness can be controlled by polymerization time. Notably, the PVal-shells retain their hollow spherical morphology upon drying, which demonstrates their intrinsic rigidity associated with the polypeptide *β*-sheets.[4, 9] The PVal-shells produced here are very different

from hollow polypeptide/polymer-based architectures (i.e., capsules) prepared by layer-by-layer (LbL) assembly, which typically exhibit 'collapsed' morphologies upon drying.[19, 32]

To further confirm that SI-ROP was responsible for the formation of hollow PVal-shells several control experiments were performed. Firstly, Val-NCA polymerization was conducted using non-functionalized silica particles; following template removal, DIC micrographs revealed the absence of stable architectures (**Figure S4A**). Similarly, the inability of APTS alone to form free-standing shells was confirmed by dissolving the silica template after silanization with APTS (**Figure S4B**). These control experiments highlight the importance of initiator-functionalized surfaces and SI-ROP in the formation of the hollow PVal-shells. Moreover, the ^{1}H NMR spectrum of the reaction supernatant after 24 h of SI-ROP only revealed the presence of unreacted Val-NCA monomers (**Figure S4C**). This demonstrates that our synthetic approach is indeed surface-confined (i.e., negligible polymerization occurred in solution).

We also investigated the possibility of tuning the size of the PVal-shells by using solid templates with different diameters. SI-ROP of Val-NCA was performed on amine-functionalised silica particles with smaller diameters (0.5 ± 0.02 μm and 1.5 ± 0.05 μm diameter) for 2 h followed by template dissolution as previously explained. SEM analysis showed the successful formation of shells with sponge-like morphologies (**Figure 3**). The formation of these PVal-shells demonstrates the ability of the present technique in creating peptide β-sheet architectures that conform readily to the 3D shape and sizes of the template.

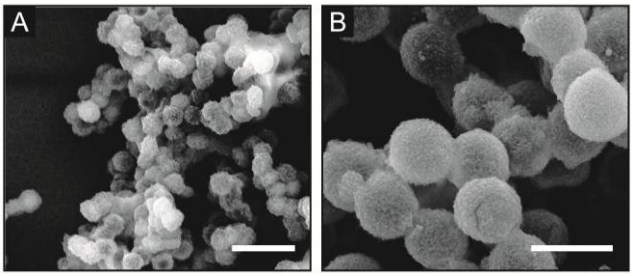

Figure 3. SEM images of PVal-shells obtained using silica particles with average diameter of A) 0.5 ± 0.02 μm and B) 1.5 ± 0.05 μm. Scale bars are 2 μm.

2.3. Stability and Degradation of PVal-Shells

The synthesised hollow PVal-shells exhibit stability at extreme pH conditions (2M HCl and 2M NaOH solution) and in the presence of protein denaturants (2M Urea and 6M Guanidine HCl (GdnCl)) (**Figure 4A**). Such stability can be attributed to the cooperative contribution of multiple non-covalent interactions throughout the architecture, namely enthalpically-driven H-bonding between the grafted PVal backbones and the entropically-driven hydrophobic interactions of the isopropyl side-chain of valine residues.[16] In addition to these interactions, the absence of ionisable groups enables the PVal grafts to remained 'interlocked' at extreme pH conditions and thus prevent dissociation or break-up of the architecture. Notably, thermal treatment of the shells in solution (i.e., 80 °C, 18 h) also did not result in disassembly since the H-bonding and hydrophobic interactions have opposing temperature-dependent energetic contributions.[16]

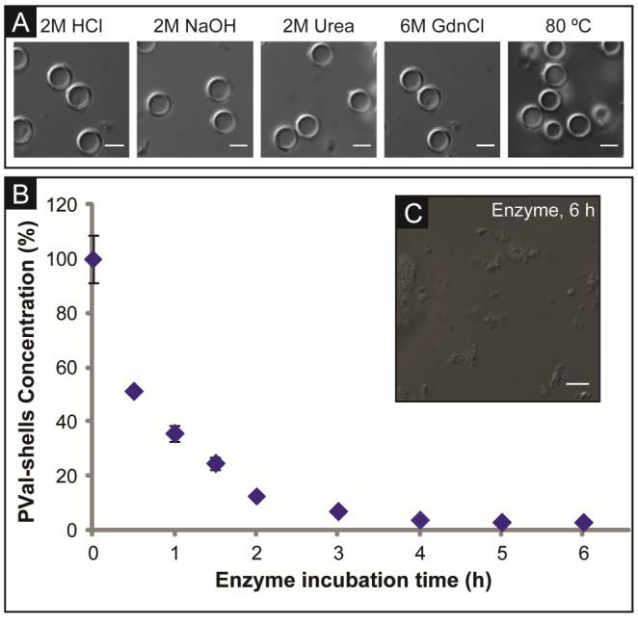

Figure 4. A) Stability of PVal-shells at extreme pH conditions (2M HCl and 2M NaOH), in the presence of typical protein denaturants (2M Urea and 6M GdnCl) and at elevated temperature (80 °C). B) Enzymatic

degradation profile of PVal-shells as characterized by flow cytometry. C) DIC micrograph of remnants of degraded PVal-shells isolated at 6 h. Scale bars are 5 μm.

However, an attractive feature of using polypeptides as building blocks is their degradability in the presence of enzymes.[2, 19] We conducted a proteolytic degradation study on the hollow PVal-shells obtained after 2 h of polymerization. During the degradation study (physiological conditions; pH 7.4 and 37 °C), the concentration of shells at different time intervals was monitored by flow cytometry. Based upon the degradation profile (**Figure 4B**), >96% of the PVal shells degraded within 6 h of incubation with the enzyme. After 6 h of incubation, DIC micrographs revealed only remnants of degraded films (**Figure 4C**).

2.3. Tailoring Functionality of Hollow Spherical Shells

2.3.1. Chain Extension

Owing to the large family of amino acids building block (natural and synthetic), peptide-based materials can potentially be engineered to display a myriad of chemical functionalities. To demonstrate the possibility of preparing shells with functional exterior layers, the β-sheet-assembled PVal films were chain-extended with either $\mathcal{E}$-carboxybenzyl-L-lysine NCA (Lys-NCA) or benzyl-L-glutamate NCA (BLG-NCA), to obtain shells composed of block copolypeptides following template dissolution. While the first block of PVal grafts are interlocked by H-bonding to provide mechanical stability, the second block introduces additional functional groups available for further covalent conjugation or biospecific interactions. Chain-extension with Lys-NCA was conducted from PVal coated silica particles (isolated after 2 h of Val-NCA SI-ROP) and stopped after 2, 4 and 24 h. After deprotection of the carboxybenzyl groups using HBr (refer to SI for experimental details), zeta potential measurements of the coated-silica particles revealed an increase from 11.0 ± 2 mV (PVal shells on silica) to 26.5 ± 5.0 mV (PVal-b-PLL, i.e. PLL brushes on PVal shells) after 24 h

chain extension with Lys-NCA (**Figure 5A**). This increase in positive surface charge is attributed to the protonated amine side-groups of the outer poly(L-lysine) (PLL) block. In comparison, when chain extension was conducted using BLG-NCA (followed by deprotection in HBr), the deprotonated acid side-groups of the poly(L-glutamic acid) (PLGA) block generate a net negative surface charge of -16.0 ± 5.2 mV (**Figure 5A**).

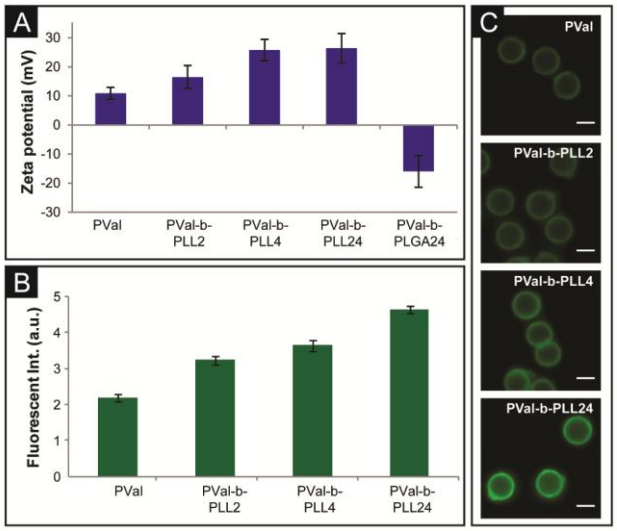

Figure 5. Change in A) surface zeta potential and B) normalized fluorescent intensity after chain extension of PVal shells with Lys-NCA and Glu-NCA to form PVal-b-PLLX and PVal-b-PLGAX shell-brush, respectively, where X denotes the polymerization time. For example, chain extension with Lys-NCA for 2 h is denoted as 'PVal-b-PLL2'. C) Fluorescence microscopy images before and after chain extension with Lys-NCA (Scale bars are 5 μm).

To study the possibility that the increase in zeta potential corresponds to thicker brushes, the amine functionalities on the PLL block were reacted with the fluorescent marker, Alexa Fluor 488 (AF488) succinimidyl ester. Following template dissolution, the isolated hollow shells grafted with PLL were analyzed using flow cytometry and fluorescence microscopy. Interestingly, the control experiment where the conjugation was conducted on PVal-shells alone (before chain extension with Lys-NCA) also showed fluorescent characteristics with a normalized fluorescence intensity (FI) of 2.2 ± 0.1 a.u. (**Figure 5B-C**).

The observed fluorescence for the PVal-shells may result from the entrapment of AF488 or conjugation of AF488 to the terminal amine groups on the PVal grafts. This is also supported by the zeta potential measurements of pure PVal shells (**Figure 5A**), which exhibit a net positive charge of 11.0 ± 2 mV, suggesting the presence of protonated amino groups at the surface of the hollow architecture. Regardless, the FI of the shells increases further to 3.2 ± 0.2 a.u. and 4.6 ± 0.1 a.u. after chain extension with Lys-NCA for 2 and 24 h, respectively (**Figure 5B-C**). The increase in FI with longer chain extension times corresponds to longer PLL segments since there would be more amine moieties available for conjugation with the AF488 marker. These experiments not only demonstrate that the *β*-sheet stabilized shells can be further functionalized, but also the degree and type of the chemical functionality can be tailored through the appropriate selection of amino acids and the period of chain extension. This provides facile access to stable multifunctional non-covalent polypeptide architectures with functionalities and properties tailored to suit desired applications.

2.3.2. Non-covalent Entrapment of Small Molecules

Analogous to the filter feeders found in nature (e.g., green mussels *Perna Viridis* and sea sponge *Hymeniacidon heliophila*),[33] the observed entrapment of AF488 dye molecules by the PVal-shells (**Figure 5B-C**), possibly as a result of hydrophobic interactions, provides a nature-inspired opportunity to potentially entrap or non-covalently conjugate other (macro)molecules to decorate the corona or walls of the PVal-shells. Therefore, we explored the capacity of the PVal-shells to encapsulate various (macro)molecules. In the first instance we demonstrated the application of the PVal-shells as catalytic supports. The PVal-shells were incubating with palladium (II) acetate ($Pd(OAc)_2$) solution and then washed thoroughly to remove any $Pd(OAc)_2$ not entrapped within the shell interior (**Figure 6**). The entrapped $Pd(OAc)_2$ was reduced *in situ* to form Pd(0) nanoparticles (PdNP) within the shells' walls. DIC microscopy and TEM analysis revealed that the shells' morphology was unaffected by

the process (**Figure S5A-B**), while higher magnification TEM images also confirmed the formation of PdNPs with diameters of 5-10 nm within the PVal shells. Using the built-in EDAX detector, the entrapped PdNP atomic content was estimated to be 1.5 wt % (**Figure S5C**).

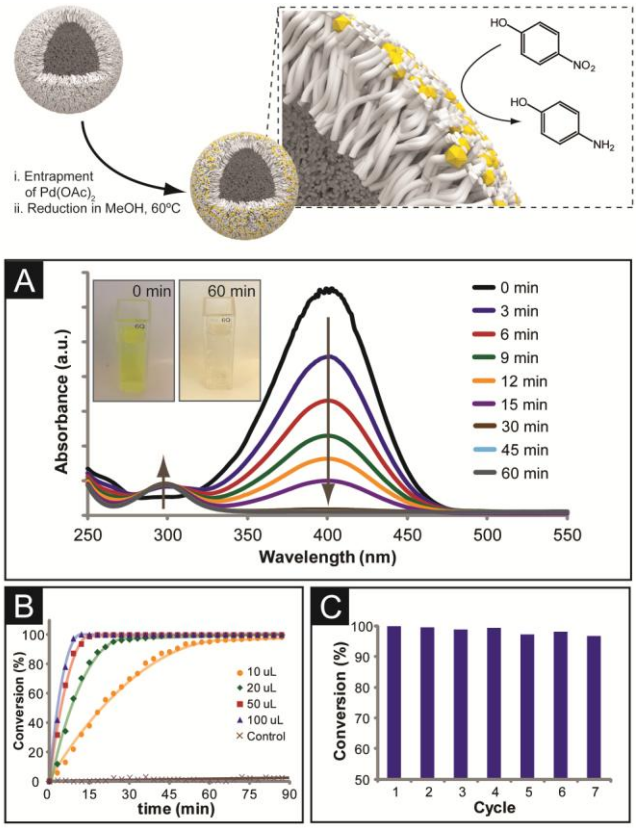

Figure 6. Formation of PVal-PdNP shells via non-covalent entrapment and *in situ* reduction. A) Evolution of absorbance spectra with increasing hydrogenation reaction time. B) Conversion kinetics of 4-NP with varying volumes of catalyst stock solution (i.e., 1 wt% suspension of PVal-PdNP shells in deionized water). Control experiment utilised PVal-shells. C) Conversion achieved in 60 min after 7 catalytic cycles.

The catalytic activity of the peptide-metal hybrid (PVal-PdNP) shells was then studied using a model reaction, specifically the Pd(0)-catalyzed reduction of 4-nitrophenol (4-NP) to 4-aminophenol (4-AP) in the presence of a reducing agent (i.e., sodium borohydride). 4-NP has a characteristic absorption at 405 nm, which was monitored overtime *via* UV-Vis spectrophotometry (**Figure 6A**).[34] Upon the introduction of the PVal-PdNP shells (10 μL of 1 wt% suspension) as catalyst, the absorption at 405 nm gradually decreases indicating the

reduction of 4-NP, which was accompanied by an increase in the 4-aminophenol absorption peak at 295 nm.[34] From the UV-Vis measurements it was determined that the reaction was 98.5 % complete after 60 min, which was also confirmed by the physical appearance of the reaction solution, which turned from yellow to colourless (**Figure 6A**). Also, by introducing more catalytic Pval-PdNP shells (i.e., 20, 50 and 100 μL of 1 wt% suspension), higher conversion of 4-NP could be achieved at faster rates (**Figure 6B**). For instance, >99% conversion was achieved after 9 minutes when 100 μL of the 1 wt% PVal-PdNP shell catalyst solution was used. Conversely, negligible catalytic conversion was observed for control experiment using PVal-shells (without entrapped PdNP). These results highlight the role of entrapped PdNP as the active catalyst and the ability to tune the reaction kinetics by adjusting the amount of PVal-PdNP shells introduced.

The application of PVal-shells as catalyst supports enables facile separation (via centrifugation) and reuse of the catalytic nanoparticles for subsequent reactions. Thus, the PVal-PdNP shells were isolated by centrifugation and washed thoroughly with deionized water before being reintroduced for the next catalytic cycle. The catalytic activity of the peptide-metal hybrid shells over 7 cycles (60 min each) was consistently high (>95%) (**Figure 6C**). The observed gradual decrease in efficiency is attributed to the loss of PVal-PdNP shells during the washing steps. These results demonstrate that the hydrophobic PVal shells can be employed to efficiently entrap inorganic nanoparticles to produce functional peptide-metal hybrid materials whilst maintaining excellent shell integrity.

2.3.3. (Simultaneous) Entrapment of Macromolecules and Drug

The entrapment capabilities of the PVal-shells towards macromolecules was studied using poly(ethylene glycol) conjugated with Alexa Fluor 647 marker (PEG647, fluoresces red) as a model. Since PEG is known to exhibit low-fouling behaviour,[35, 36] human serum albumin protein tagged with fluorescent marker Alexa Fluor 488 (HSA488, fluoresces green)

was chosen to assess the effective non-covalent interaction between PVal-shells and PEG647. Fluorescence microscopy images and FI (as quantified by flow cytometry) of PVal-shells incubated with HSA488 indicate significant adsorption of the protein with a normalized FI of 60.3 ± 0.7 a.u. (**Figure 7A & 7C**). This result is expected as the HSA protein would foul the shells' surface via H-bonding and/or non-specific hydrophobic interactions.[37] In contrast, the adsorption of HSA488 on PVal shells that were previously PEGylated through non-covalent conjugation of PEG647 was significantly reduced (normalized FI of 9.3 ± 0.3 a.u.; reduction of 85%) (**Figure 7B & 7C**). This confirms the successful PEGylation of the corona of PVal-shells. To investigate the conjugation mechanism, a control experiment was conducted with non-functionalized PEG (without hydrophobic dye tail) followed by incubation with HSA488. The resulting FI (53.9 ± 1.4 a.u.) only corresponds to a 10% reduction in HSA488 fouling (**Figure 7C**), indicating the limited entrapment of PEG. This demonstrates that the driving force for conjugation of PEG647 most likely results from hydrophobic interactions between the PVal shell and the hydrophobic tail of PEG647 (Alexa Fluor 647 moiety). This mechanism presents a facile approach to coordinate a wide range of macromolecules/polymers with hydrophobic anchors.

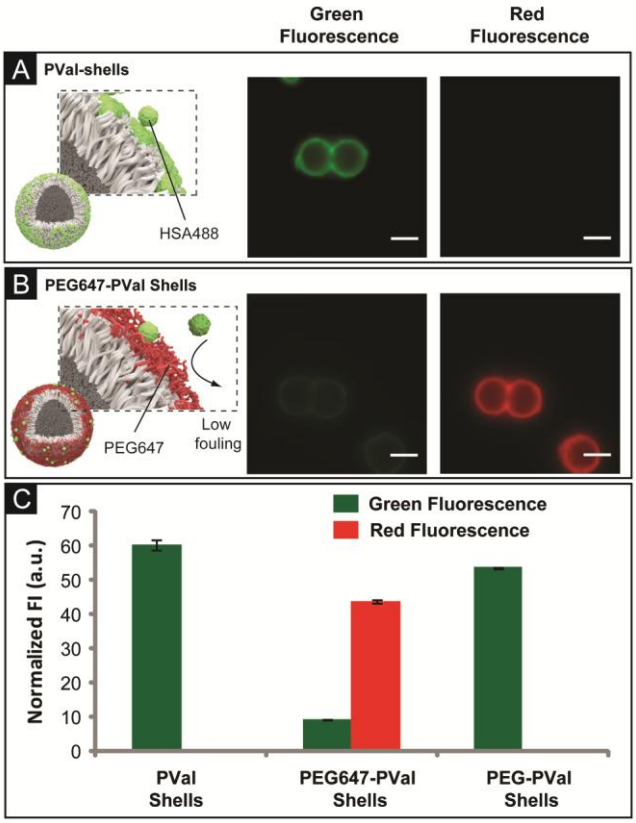

Figure 7. Fluorescence microscopy images indicating A) adsorption of HSA-AF488 on PVal-shells and B) low-fouling behaviour of PEGylated PVal-shells. C) Normalized fluorescence intensity of PVal and PEG-PVal shells as measured by flow cytometry. Scale bar is 5 μm.

Another unique feature of the hollow PVal-shells is the ability to trap multiple (macro)molecules. This ability is particularly important in the design of multi-modal drug delivery vectors where efficacy depends on the successful encapsulation and delivery of therapeutics, and specific *in vivo* biointeractions.[35] To demonstrate the utility of the PVal-assembles as potential platforms for multifunctional therapeutic carriers, SI-ROP of Val-NCA was performed from APTS-functionalized mesoporous silica templates. Following template dissolution, the *β*-sheet-assembled PVal negative-replicas were incubated in a doxorubicin (DOX) solution followed by a PEG488 solution (PEG conjugated with AF488, fluoresces green) (**Figure S6**). While DOX serves as the model encapsulated cargo, the low-fouling PEGylated corona is potentially crucial to improve *in vivo* biodistribution.[35] Fluorescence

microscopy and flow cytometry indicated the successful encapsulation of DOX with normalized FIs of 14.5 ± 0.6 a.u. at 488 nm (green) and 31.5 ± 0.8 a.u. at 570 nm (red) (**Figure S6C**). After the subsequent incubation with PEG488, the normalized FI at 488 nm increases to 22.5 ± 1.6 a.u. while the FI at 570 nm remains constant (32.0 ± 1.3 a.u.) (**Figure S6C**), demonstrating absorption of the PEG488 to the shell. Also, multiple (macro)molecules can be non-covalently conjugated to the resultanting particles, which provides convenient opportunities for the nature-inspired fabrication of multifunctional materials tailored for specific needs.

3. Conclusion

In summary, we have demonstrated the application of SI-ROP as a simple, rapid and robust bottom-up surface-confined synthetic approach that enables the formation of novel well-defined β-sheet-assembled materials with tailored dimensions. As an initial proof of concept, we performed SI-ROP of Val-NCA from amine-functionalized spherical silica particles and demonstrated that parallel β-sheets were formed within 15 minutes of polymerization. Upon dissolution of the silica template, the resulting β-sheet conformation acts as a non-covalent stabilization force, leading to the formation of spherical, enzyme-degradable porous PVal-shells that exhibit sponge-like morphology. The wall thickness of the PVal-shells can be tuned by varying the polymerization time, while additional chemical functionalities can be introduced by simple chain extension reactions. Furthermore, we report the unique properties of these free-standing shells for the nature-inspired non-covalent entrapment and conjugation of various materials ranging from metal nanoparticles, to synthetic polymers, to intercalating drug molecules and protein. Overall, the combination of surface-initiated polymerization and non-covalent binding provides a powerful and versatile synthetic approach towards the development of multifunctional and compartmentalized (bio)materials. This surface-driven approach may potentially be applicable to the formation of

other unique β-sheet-assembled nano/micro-architectures, depending on the shape and size of the template employed. Current work is directed at investigating this possibility, as well as utilizing the reported hollow PVal-shells as platforms for organic catalysis and theranostic devices.

4. Experimental Section

4.1. Materials

H-Val-OH, H-Glu(OBzl)-OH, and H-Lys(Z)-OH were obtained from Bachem and used as received. Triphosgene (98%), (3-aminopropyl)triethoxysilane (APTS) (98%), hydrofluoric acid (48 wt% in H_2O), *n*-pentane (anhydrous, >99%), hydrobromic acid (33 % in acetic acid), pottasium bromide (KBr) (>99%), phosphate buffered saline (PBS) tablets, 2,2,2-trifluoroethanol (TFE) (>99%), palladium (II) acetate ($Pd(OAc)_2$) (>99.9%), human serum albumin (HSA) (lyophilized powder, >97%), protease from bovine pancreas (type I, >5 units/ mg solid), benzylamine (99%), doxorubicin hydrochloride (DOX) (>98%), 4-(4,6-dimethoxy-1,3,5-triazin-2-yl)-4-methylmorpholinium chloride (DMTMM) (>96%), sodium borohydride (>99%) and 4-nitrophenol (>99%) were purchased from Sigma-Aldrich and used as received. Alexa Fluor 488 cadaverine, Alexa Fluor 488 carboxylic acid, succinimidyl ester and Alexa Fluor 647 carboxylic acid, succinimidyl ester were purchased from Invitrogen and were used as received. Methoxy-PEG(5kDa)-amine (HCl salt) was purchased from Jenkem Technology USA and used as received. Ammonium fluoride (Fluka, 40% in H_2O), anhydrous *N*,*N*-dimethylformamide (DMF) (Acros Organics, extra dry, >99.8%), tetrahydrofuran (THF) (Honeywell, 99.9%, HPLC grade) and sulphuric acid (H_2SO_4) (Scharlau, 99%) were used as received. *n*-Hexane (99%), sodium chloride (NaCl) (99%), hydrogen peroxide (H_2O_2) (30%), isopropanol (IPA) (99%), *N*,*N*-dimethylformamide (DMF) (98%), chloroform (99.8%) and methanol (98%) were purchased from Chem-Supply and used as received. Anhydrous and deoxygenated THF was obtained by distillation under argon from sodium benzophenone ketyl.

Deuterated dimethylsulfoxide (d_6-DMSO) was purchased from Cambridge Isotope Laboratories and used as received. High-purity water (Milli-Q) with a resistivity greater than 18 MΩ.cm was obtained from anin-line Millipore RiOs/Origin water purification system. Nonporous silica particles (5 wt% suspensions) were purchased from Microparticles GmbH (Berlin, Germany). Mesoporous silica (average diameter 7 μm, D40/D90 < 1.35, 100 nm pore size) were purchased from DAISO Co. Ltd. and dissolved in Milli-Q water to afford 1 wt% suspension before use. Silicon wafers (MMRC Pty. Ltd., Melbourne, Australia) were cut into *ca.* 1 × 1 cm squares and cleaned with Piranha solution (sulphuric acid: hydrogen peroxide = 7:3) – *caution! Piranha solution is highly corrosive and extreme care should be taken during preparation and use*. The wafers were then sonicated in isopropanol:water (1:1) solution for 20 min followed by soaking in RCA solution (water: ammonia: hydrogen peroxide = 5:1:1) for another 20 min at 60 °C. The wafers were thoroughly washed with Milli-Q after each step.

4.2. Characterization Methods

Nuclear Magnetic Resonance (NMR): Proton (^{1}H) and carbon (^{13}C) NMR spectroscopy was conducted using a Varian Unity 400 MHz spectrometer operating at 400 MHz and 100 MHz, respectively. Deuterated dimethyl sulfoxide (d_6-DMSO) was used as the solvent and samples were prepared at a concentration of *ca.* 20 mg mL^{-1}.

Differential interference contrast (DIC) and Fluorescent microscopy images of polypeptide coated particles and hollow polypeptide shells were taken with an Olympus IX71 digital wide-field inverted microscope equipped with DIC slider (U-DICT, Olympus), a 60× oil immersion objective (Olympus UPFL20/0.5NA, W.D. 1.6), a UF1032 fluorescence filter cube and the corresponding filter sets. A CCD camera was mounted on the left-hand port of the microscope and a tungsten lamp was used for DIC images.

Flow cytometry: Fluorescence intensity histograms of fluorescently labelled shells were acquired using Partec CyFlow Space instrument using an excitation wavelength of 488 and 544 nm. Data analysis was performed with Partec CyFlowMax software and the normalized fluorescence intensities were obtained from the histograms.

Zetasizer Nano ZS (Malvern Instruments): were used to measure the zeta potential measurements of the peptide-coated silica particles. 1 mL of peptide-coated particles (0.05 wt% in Milli-Q water) was placed in a disposable zeta cell and zeta potential measurements were conducted at 20 °C. Three independent measurements were conducted for each sample and data analysis was performed with Dispersion Tehcnology Software V5.03 provided by Malvern Instruments.

Transmission Electron Microscopy (TEM): was used to image dried shells. 1 uL of concentrated hollow shells solution was deposited on TEM grids. TEM analysis was carried out with a Tecnai F30 transmission electron microscope operating at 120 kV. Elemental analysis at a line across the shells was performed in scanning TEM (STEM) mode using an EDAX X-ray detector.

Fourier Transform Infrared Spectroscopy (FT-IR): was performed on Bruker Tensor 27 with mid-infrared range (400-4000 cm^{-1}). The instrument was equipped with OPUS 6.5 Software and GladiATR™ with monolithic diamond ATR from Pike Technologies. Typically, 0.1 mg of coated particles/ dried shells sample were ground with dry potassium bromide (KBr) at approximately 1 wt% and the resulting powder was pressed into a transparent pellet using Specac 10 ton Hydraulic Press. For each sample, 100 scans were taken in transmission mode at a resolution of 2 cm^{-1}.

UV Spectrophotometry: UV absorbance spectra were obtained using Shimadzu UV-1800 Spectrophotometer and UVProbe software package. The wavelength range of 250-550 nm was selected with medium scan speed and sampling interval of 1 nm. Scan mode was set to 21 repeats with 3 minutes interval between scans.

X-ray Diffraction (XRD): was performed using Bruker D8 Advance instrument with CuKα radiation (40 kV, 40 mA) and a nickel filter. Diffraction patterns were collected in the 2θ range of 5 to 55° with a step size of 0.04° and 14 seconds/ step.

4.3. Experimental Procedures

Synthesis of α-amino acid NCA derivatives: α-amino acid NCA derivatives were synthesized as previously reported in the literature.[11, 19]

L-Val NCA (Val-NCA): ^{1}H NMR (400 MHz, d_6-DMSO): δ_H 0.82–0.84 (*d*, 3H, *J* = 7.0 Hz, 1 C**H**$_3$), 0.91–0.93 (*d*, 3H, *J* = 7.2 Hz, 1 C**H**$_3$), 1.97–2.08 (*m*, 1H, 1 C**H**), 4.32 (*dd*, 1H, *J* = 1.2 & 4.0 Hz, C**H**N), 9.06 (*br s*, 1H, 1 N**H**) ppm. ^{13}C NMR (100 MHz, d_6-DMSO): δ_C 17.0 (**C**H$_3$), 30.5 (**C**H), 56.9 (**C**HN), 63.0 (**C**H$_2$N), 152.5 (NH**C**O$_2$), 170.0 (**C**H**C**O$_2$) ppm.

Benzyl-L-glutamate NCA (Glu-NCA): ^{1}H NMR (400 MHz, d_6-DMSO): δ_H 1.87–2.10 (*m*, 2H, C**H**$_2$), 2.52 (*t*, 2H, *J* = 7.6 Hz, C**H**$_2$), 4.45 (*dd*, 1H, *J* = 5.6 & 8.0 Hz, C**H**N), 5.10 (*s*, 2H, C**H**$_2$O), 7.31–7.40 (*m*, 5H, Ar**H**), 9.09 (*s*, 1H, N**H**) ppm. ^{13}C NMR (100 MHz, d_6-DMSO): δ_C 26.3 (**C**H$_2$), 29.0 (**C**H$_2$), 56.1 (**C**HN), 65.6 (**C**H$_2$), 127.9 (3 Ar**C**H), 128.4 (2Ar**C**H), 135.9 (Ar**C**C), 151.8 (NH**C**O$_2$), 171.2 (**C**H**C**O$_2$), 171.6 (**C**H$_2$**C**O$_2$) ppm.

ε-Carboxybenzyl-L-Lysine NCA (Lys-NCA): ^{1}H NMR (400 MHz, d_6-DMSO): δ_H 1.22–1.45 (*m*, 4H, 2 C**H**$_2$), 1.60–1.77 (*m*, 2H, 1 C**H**$_2$), 3.01 (*q*, 2H, *J* = 6.0 Hz, C**H**$_2$N), 4.42 (*t*, 1H, *J* = 6.0 Hz, C**H**N), 5.00 (*s*, 2H, C**H**$_2$O), 7.25–7.38 (*m*, 5H, 5 Ar**H**), 9.11 (*br s*, 2H, 2 N**H**) ppm.

^{13}C NMR (100 MHz, d_6-DMSO): δ_C 21.5 (**C**H_2), 28.7 (**C**H_2), 30.6 (**C**H_2), 56.9 (**C**HN), 65.0 (**C**H_2N), 127.6 (3 Ar**C**H), 128.2 (2 Ar**C**H), 137.1 (Ar**CC**), 151.8 (NH**C**O_2), 156.0 (NH**C**O_2), 171.5 (**C**H**C**O_2) ppm.

Synthesis of Poly(L-Valine) (PVal) Hollow Shells: Amine-functionalised particles were prepared using an APTS silanization method reported in the literature.[19, 38] A suspension of aminated particles (1 mL, 1.0 wt% in anhydrous DMF) were centrifuged (3300 rcf) and the solvent removed prior to the addition of Val-NCA monomer solutions (1 mL, 0.75 M in anhydrous DMF). The tubes were sealed and the particles suspended at 20 °C with constant agitation for a specified period of time ranging from 15 min to 24 h. After the specified reaction period, the supernatant was removed and the PVal-coated particles were washed with DMF (3 × 1 mL) and sonicated in DMF (1 mL) for 30 min. To remove potential non-grafted materials, the coated particles were then washed with THF (3 × 1 mL) and chloroform (3 × 1 mL) and were resuspended with constant agitation in trifluoroethanol solution (10 vol% in chloroform) for 18 h at 20 °C. Finally, the suspension was sonicated for 10 min and washed with chloroform (3 × 1 mL), THF (3 × 1 mL), DMF (3 × 1 mL) and Milli-Q (3 × 1 mL). The silica templates were then removed by the addition of 250 μL of 2 M HF/8 M NH_4F solution (pH 5.0). After 2 min, the hollow PVal architectures were washed with Milli-Q water (3 × 1 mL) and then stored in Milli-Q water (1 mL) prior to analysis.

Synthesis of Block-copolypeptide Hollow Shells: PVal-coated silica particles (1 mL, 1.0 wt%) isolated after 2 h of SI-ROP were washed with anhydrous DMF (3 × 1 mL) to remove unreacted monomers and non-grafted materials. After centrifugation (3300 rcf), a solution of Glu-NCA or Lys-NCA (1 mL, 0.75 M in anhydrous DMF) was added to the PVal coated particles and allowed to react for a specified period of time ranging from 2 to 24 h followed

by thorough washing with DMF (3 × 1 mL) and Milli-Q water (3 × 1 mL). Deprotection of the benzyl protecting groups was performed by the addition of HBr solution (300 µL, 33 % in acetic acid) to the coated particles, followed by continuous agitation for 12 h. Excess HBr and by-products were then removed by washing with Milli-Q water (3 × 1 mL). Dissolution of the template was then performed as previously described.

Proteolytic Degradation of Hollow PVal-shells: PVal-shells isolated after 2 h of ROP and HF treatment were washed with PBS buffer (pH 7.4, 3 × 1 mL) and resuspended in 1 mL of PBS. The shells' concentration was determined by flow cytometry and was adjusted to 150,000 shells/mL through dilution in PBS buffer. 1 mL of shells stock solution was centrifuged (3300 rcf, 10 min), the supernatent removed and a solution of protease 2 mg/mL in pH 7.4 PBS buffer (1 mL, 37 °C) was added. An aliquot was immediately drawn to count the initial number of shells (t = 0 min). The suspension was agitated at 37 °C and aliquots were taken after specified periods for flow cytometry measurements. Three flow cytometry measurements were conducted for each time point and the degradation experiment was repeated twice. Aliquots containing degraded shells (6 h) were taken for observation via DIC microscopy.

PEGylation of PVal-shells and HSA Fouling Characteristics: Hollow PVal-shells isolated after 2 h of SI-ROP and HF treatment were washed with Milli-Q water (3 × 1 mL). After centrifugation (2 min, 3300 rcf), the shells were incubated in PEG647 solution (5 kDa methoxy PEG conjugated with Alexa Fluor 647 dye) (1 mL, 1 mg/mL in Milli-Q water) for 1 h under constant agitation. Afterwards, the PEGylated shells were thoroughly washed with Milli-Q water until the supernatant lacked any UV absorbance (i.e., all unbound PEG was removed). The PEGylated PVal-shells were then resuspended in 1 mL HSA488 (human serum albumin conjugated with Alexa Fluor 488 dye) for 1 h under constant agitation. The

PEG-PVal-shells were thoroughly washed again with Milli-Q water until any unbound HSA488 was removed. Fluorescence microscopy was then used to observe the shells fluorescence at 488 and 647 nm. Normalized fluorescent intensities at these wavelengths were then determined by flow cytometry (three measurements were conducted). As control experiments, PVal-shells incubated only with PEG647 or HSA488 (same conditions as above) were also analyzed with fluorescence microscopy and flow cytometry. ***Note****: PEG647 fluoresces red while HSA488 fluoresces green.*

Non-covalent entrapment and In Situ Formation of Pd(0) Nanoparticles: PVal-shells isolated after 2 h of SI-ROP and HF treatment were washed with DMF (3 × 1 mL) and then a solution of $Pd(OAc)_2$ (1 mL, 1 mg/mL $Pd(OAc)_2$ in DMF) was added and incubated under constant agitation for 1 h (20 °C). The shells were then washed with DMF (6 × 1 mL) to remove unbound $Pd(OAc)_2$ and were introduced into an alcohol environment by washing with methanol (3 × 1 mL). The $Pd(OAc)_2$-entrapped PVal-shells were then resuspended in methanol (1 mL) and heated up to 60 °C under constant agitation. After 18 h of reduction, the previously yellowish suspension turned to dark grey indicating the *in situ* formation of Pd(0) nanoparticles. The Pd(0)-entrapped PVal (PVal-PdNP) shells were then washed with methanol (3 × 1 mL) and Milli-Q water (3 × 1 mL) before observation via DIC microscopy and TEM.

Pd-catalyzed Reduction of 4-Nitrophenol: Stock solutions of 4-nitrophenol (5 mM in Milli-Q water) and sodium borohydride (0.2 M in Milli-Q water) were freshly prepared prior to the experiment. 0.1 mL of the 4-nitrophenol solution and 1 mL of the sodium borohydride solution were then added into a quartz cuvette containing Milli-Q (2 mL). 10 µL of the PVal-PdNP shell suspension (1 wt%) were then introduced and the absorption spectrum was acquired at 3 min intervals using a UV-VIS spectrophotometer to monitor catalytic

conversion. After 60 min, the shells were isolated via centrifugation (2800 rcf, 10 min) and washed with Milli-Q water (3 × 1 mL) before being resuspended in 50 μL Milli-Q water and reintroduced for the next catalytic cycle.

Entrapment of PEG and DOX in Mesoporous PVal Matrices: PVal-coated mesoporous silica was obtained by the silanization and SI-ROP procedures previously described. After HF treatment (1 mL of 2 M HF/8 M NH_4F solution), the PVal particle matrices were immersed in doxorubicin hydrochloride (DOX) solution (1 mL, 1 mg/mL in Milli-Q water) for 1 h with constant agitation. Unbound DOX was then removed through repeated washing with Milli-Q water (*ca.* 10 x 1 mL), until the supernatant lacked any UV absorbance. The DOX-entrapped PVal matrices were then incubated in PEG488 solution (1 mL, 1 mg/mL PEG488 in Milli-Q water) for 1 h under constant agitation. Free PEG488 was removed by thorough washing with Milli-Q water (10 × 1 mL), until the supernatant lacked any UV absorbance. Successful entrapment was determined by fluorescence microscopy and flow cytometry. ***Note****: DOX shows fluorescence at both 488 and 570nm (green and red, respectively) while PEG488 only shows green fluorescence*

Supporting Information
Supporting Information is available from the Wiley Online Library or from the author.

Acknowledgements
The authors acknowledge the Australian Research Council under Future Fellowship (FT110100411, G.G.Q.) scheme for financial support of this work. We also thank Dr. Matthew Rowles for the assistance with XRD, Ka Noi for the assistance with HF treatment.

Received: ((will be filled in by the editorial staff))
Revised: ((will be filled in by the editorial staff))
Published online: ((will be filled in by the editorial staff))

Reference

[1] H. R. Kricheldorf, Angewandte Chemie International Edition 2006, 45, 5752.

[2] S. H. Wibowo, A. Sulistio, E. H. H. Wong, A. Blencowe, G. G. Qiao, Chemical Communications 2014, 50, 4971.
[3] T. J. Gill, D. S. Papermaster, J. F. Mowbray, Nature 1964, 203, 644; N. Koga, R. Tatsumi-Koga, G. Liu, R. Xiao, T. B. Acton, G. T. Montelione, D. Baker, Nature 2012, 491, 222.
[4] S. Ling, C. Li, J. Adamcik, Z. Shao, X. Chen, R. Mezzenga, Advanced Materials 2014, n/a.
[5] H.-J. Jin, D. L. Kaplan, Nature 2003, 414, 1057; B. A. Lawrence, C. A. Vierra, A. M. F. Moore, Biomacromolecules 2004, 5, 689.
[6] J. H. Ortony, C. J. Newcomb, J. B. Matson, L. C. Palmer, P. E. Doan, B. M. Hoffman, S. I. Stupp, Nat Mater 2014, advance online publication; L. E. R. O'Leary, J. A. Fallas, E. L. Bakota, M. K. Kang, J. D. Hartgerink, Nat Chem 2011, 3, 821; L. Finegold, J. L. Cude, Nature 1972, 238, 38.
[7] S. Zhang, M. A. Greenfield, A. Mata, L. C. Palmer, R. Bitton, J. R. Mantei, C. Aparicio, M. O. de la Cruz, S. I. Stupp, Nat Mater 2010, 9, 594.
[8] A. Sinaga, T. A. Hatton, K. C. Tam, Biomacromolecules 2007, 8, 2801.
[9] E. T. Pashuck, H. Cui, S. I. Stupp, Journal of the American Chemical Society 2010, 132, 6041.
[10] R. F. Epand, H. A. Scheraga, Biopolymers 1968, 6, 1551; S. L. Goh, A. P. Platt, K. E. Rutledge, I. Lee, Journal of Polymer Science Part A: Polymer Chemistry 2008, 46, 5381.
[11] S. H. Wibowo, A. Sulistio, E. H. H. Wong, A. Blencowe, G. G. Qiao, Australian Journal of Chemistry 2014, 67, 598.
[12] J. D. Hartgerink, E. Beniash, S. I. Stupp, Science 2001, 294, 1684.
[13] J. Zou, F. Zhang, Y. Chen, J. E. Raymond, S. Zhang, J. Fan, J. Zhu, A. Li, K. Seetho, X. He, D. J. Pochan, K. L. Wooley, Soft Matter 2013, 9, 5951.
[14] R. C. Claussen, B. M. Rabatic, S. I. Stupp, Journal of the American Chemical Society 2003, 125, 12680.
[15] A. Mata, Y. Geng, K. J. Henrikson, C. Aparicio, S. R. Stock, R. L. Satcher, S. I. Stupp, Biomaterials 2010, 31, 6004; D. A. Harrington, E. Y. Cheng, M. O. Guler, L. K. Lee, J. L. Donovan, R. C. Claussen, S. I. Stupp, Journal of Biomedical Materials Research Part A 2006, 78A, 157; N. L. Angeloni, C. W. Bond, Y. Tang, D. A. Harrington, S. Zhang, S. I. Stupp, K. E. McKenna, C. A. Podlasek, Biomaterials 2011, 32, 1091.
[16] J. D. Hartgerink, J. R. Granja, R. A. Milligan, M. R. Ghadiri, Journal of the American Chemical Society 1996, 118, 43.
[17] R. Chapman, M. Danial, M. L. Koh, K. A. Jolliffe, S. Perrier, Chemical Society Reviews 2012, 41, 6023.
[18] V. Kozlovskaya, J. F. Alexander, Y. Wang, T. Kuncewicz, X. Liu, B. Godin, E. Kharlampieva, ACS Nano 2014, 8, 5725; O. Shimoni, Y. Yan, Y. Wang, F. Caruso, ACS Nano 2012, 7, 522.
[19] S. H. Wibowo, E. H. H. Wong, A. Sulistio, S. N. Guntari, A. Blencowe, F. Caruso, G. G. Qiao, Advanced Materials 2013, 25, 4619.
[20] S. Lifson, C. Sander, Nature 1979, 282, 109.
[21] M. S. Lamm, K. Rajagopal, J. P. Schneider, D. J. Pochan, Journal of the American Chemical Society 2005, 127, 16692; C. Zhou, B. Leng, J. Yao, J. Qian, X. Chen, P. Zhou, D. P. Knight, Z. Shao, Biomacromolecules 2006, 7, 2415.
[22] R. Al-Oweini, H. El-Rassy, Journal of Molecular Structure 2009, 919, 140; E. Soto-Cantu, S. Turksen-Selcuk, J. Qiu, Z. Zhou, P. S. Russo, M. C. Henk, Langmuir 2010, 26, 15604.

[23] M. I. Gibson, N. R. Cameron, Angewandte Chemie International Edition 2008, 47, 5160.
[24] T. Miyazawa, Y. Masuda, K. Fukushima, Journal of Polymer Science 1962, 62, S62.
[25] T. Miyazawa, E. R. Blout, Journal of the American Chemical Society 1961, 83, 712.
[26] A. Rösler, H.-A. Klok, I. W. Hamley, V. Castelletto, O. O. Mykhaylyk, Biomacromolecules 2003, 4, 859.
[27] N. H. Lee, L. M. Christensen, C. W. Frank, Langmuir 2003, 19, 3525.
[28] T. Kōmoto, K. Y. Kim, M. Ōya, T. Kawai, Die Makromolekulare Chemie 1974, 175, 283.
[29] M. Tsutsumi, J. M. Otaki, Journal of Chemical Information and Modeling 2011, 51, 1457.
[30] P. Papadopoulos, G. Floudas, H. A. Klok, I. Schnell, T. Pakula, Biomacromolecules 2003, 5, 81.
[31] A. O. Moughton, R. K. O'Reilly, Chemical Communications 2010, 46, 1091.
[32] H. Ejima, J. J. Richardson, K. Liang, J. P. Best, M. P. van Koeverden, G. K. Such, J. Cui, F. Caruso, Science 2013, 341, 154; J. Guo, Y. Ping, H. Ejima, K. Alt, M. Meissner, J. J. Richardson, Y. Yan, K. Peter, D. von Elverfeldt, C. E. Hagemeyer, F. Caruso, Angewandte Chemie International Edition 2014, 53, 5546.
[33] D. Batista, K. Tellini, A. H. Nudi, T. P. Massone, A. d. L. Scofield, A. d. L. R. Wagener, Marine Environmental Research 2013, 92, 234; W.-X. Wang, A. T. S. Chow, Environmental Toxicology and Chemistry 2002, 21, 451.
[34] G. Marcelo, A. Muñoz-Bonilla, M. Fernández-García, The Journal of Physical Chemistry C 2012, 116, 24717.
[35] Z. Poon, D. Chang, X. Zhao, P. T. Hammond, ACS Nano 2011, 5, 4284.
[36] I. Banerjee, R. C. Pangule, R. S. Kane, Advanced Materials 2011, 23, 690.
[37] S. N. Guntari, E. H. H. Wong, T. K. Goh, R. Chandrawati, A. Blencowe, F. Caruso, G. G. Qiao, Biomacromolecules 2013, 14, 2477.
[38] T. Borase, M. Iacono, S. I. Ali, P. D. Thornton, A. Heise, Polymer Chemistry 2012, 3, 1267.

Table of Contents Entry

Keyword: Peptide *β*-sheet Polymerization

Steven Harris Wibowo, Adrian Sulistio, Edgar H. H. Wong, Anton Blencowe and Greg G. Qiao*

Functional and Well-defined *β*-sheet-assembled Porous Spherical Shells by Surface-guided Peptide Formation

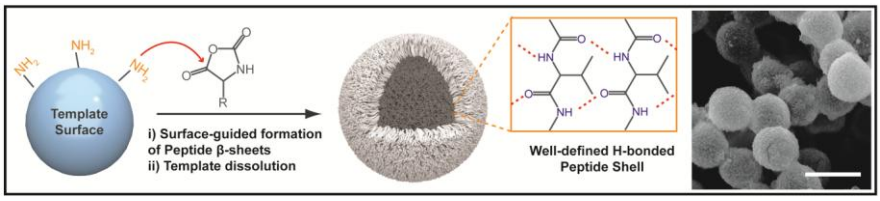

Get in shape: Well-defined peptide *β*-sheet-assembled porous shells with tailored dimensions were prepared by a simple, rapid and robust bottom-up strategy involving surface-initiated ring-opening polymerisation. Further exploitation of the hollow shells demonstrates the ability to non-covalently entrap small molecules, nanoparticles, proteins, drugs and polymers to form functional materials for various potential applications.

Supporting Information

Functional and Well-defined *β*-sheet-assembled Porous Spherical Shells by Surface-guided Peptide Formation

*Steven Harris Wibowo, Adrian Sulistio, Edgar H. H. Wong, Anton Blencowe and Greg G. Qiao**

S. H. Wibowo, Dr. Adrian Sulitio, Dr. Edgar H. H. Wong and Prof. G. G. Qiao
Dept. Chemical and Biomolecular Engineering
The University of Melbourne,
Parkville, VIC 3010, Australia
E-mail: gregghq@unimelb.edu.au

Dr. A. Blencowe
Division of Information Technology, Engineering and the Environment
University of South Australia
Mawson Lakes, SA 5095, Australia

Supplementary Figures

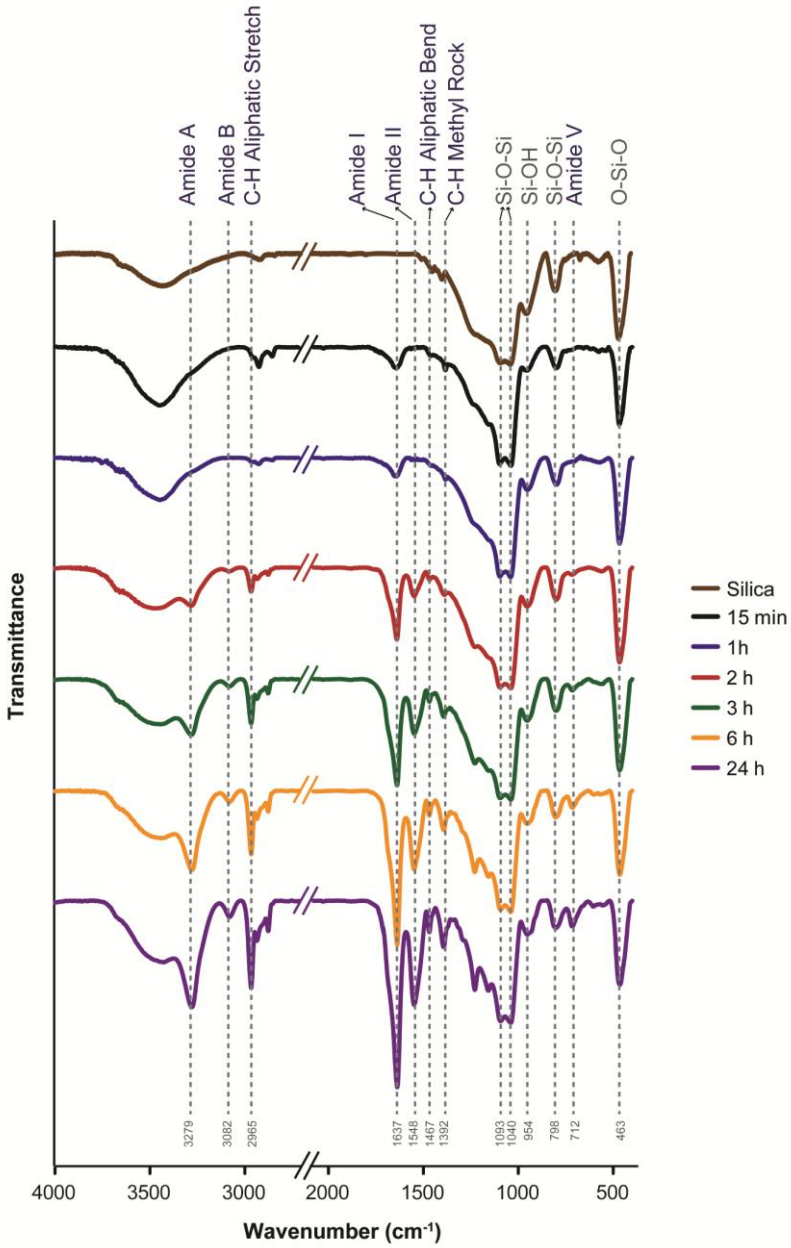

Figure S1. FT-IR spectra of bare and PVal-coated silica particles isolated after terminating the SI-ROP at different predetermined times.

Table S1. Location of Amide bands and Si-O-Si asymmetric stretches from FT-IR spectra of PVal-coated silica particles. Ratio of Amide I/Si-O peak areas were obtained by deconvolution of the FT-IR spectra using a Lorentzian fit.

ROP Time	Amide I (cm^{-1})	Amide II (cm^{-1})	Amide V (cm^{-1})	Amide A (cm^{-1})	Amide B (cm^{-1})	Si-O-Si Asymmetric stretch	Amide I /Si-O ratio
15 min	1640	-*	-*	-*	-*	1098, 1040	0.02
1 h	1640	-*	-*	-*	-*	1097, 1041	0.02
2 h	1638	1546	714	3285	-*	1096, 1040	0.11
3 h	1637	1547	714	3283	3083	1096, 1040	0.19
6 h	1637	1548	714	3279	3083	1096, 1040	0.31
24 h	1637	1548	714	3279	3082	1094, 1040	0.79

* Weak or no band observed

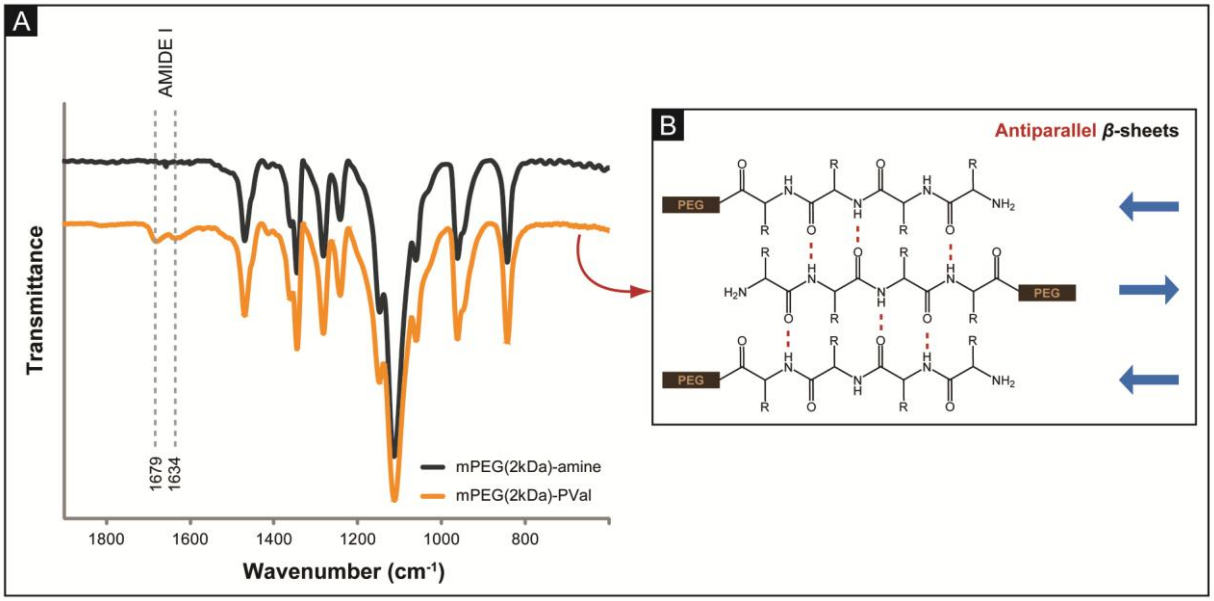

Figure S2. A) FT-IR spectra of mPEG(2kDa)-amine and m-PEG(2kDa)-PVal. B) Schematic illustration of the antiparallel *β*-sheet conformation adopted by mPEG(2kDa)-PVal.

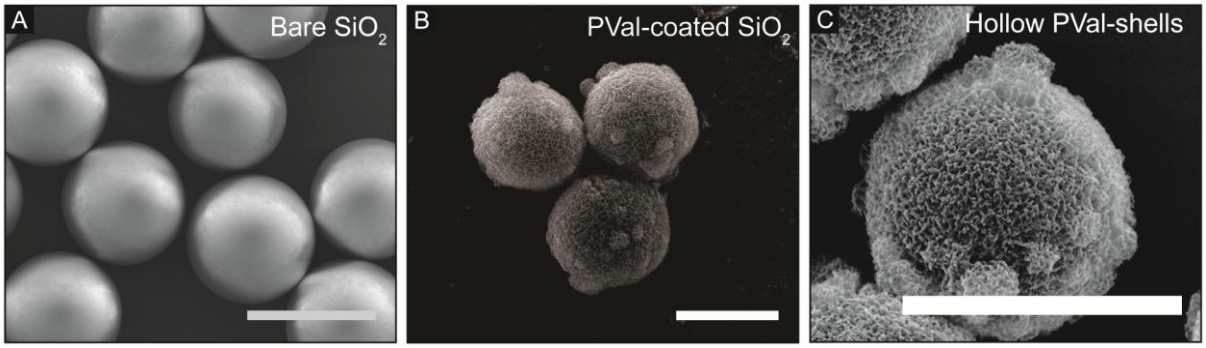

Figure S3. SEM images of A) bare silica particles showing average particle diameter of 5 µm. B) After 2h SI-ROP, the diameter of PVal-coated silica increases to 5.4 µm, indicating PVal shell thickness of approx. 200 nm. C) Following subsequent HF treatment, the hollow PVal-shells shrink to 4.4 µm. The wall thickness and shrinkage corroborates the TEM results (Figure S5). Scale bars are 5 µm.

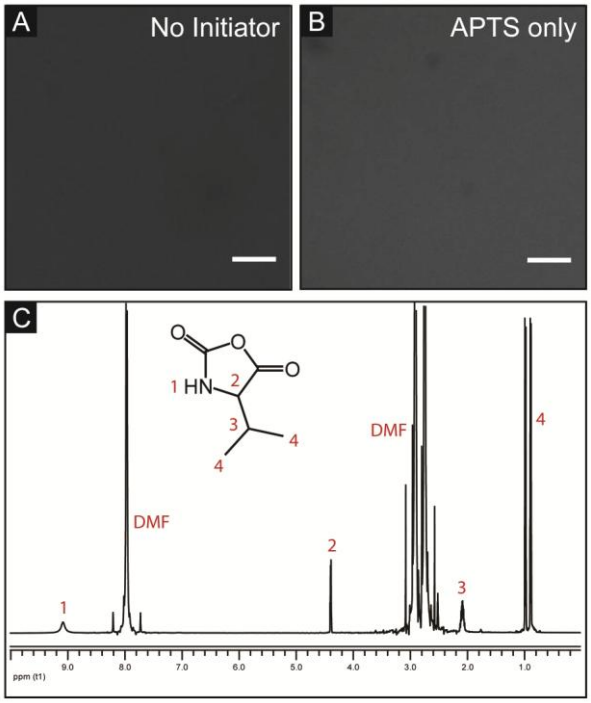

Figure S4. DIC microscopy images showing: A) the absence of PVal-shells when no APTS silanization was performed (bare silica surface as initiator); B) that silica particles modified with APTS alone do not form free-standing architectures after template dissolution. C) ^{1}H-NMR of reaction supernatant after 24 h of SI-ROP revealing only unreacted Val-NCA monomer.

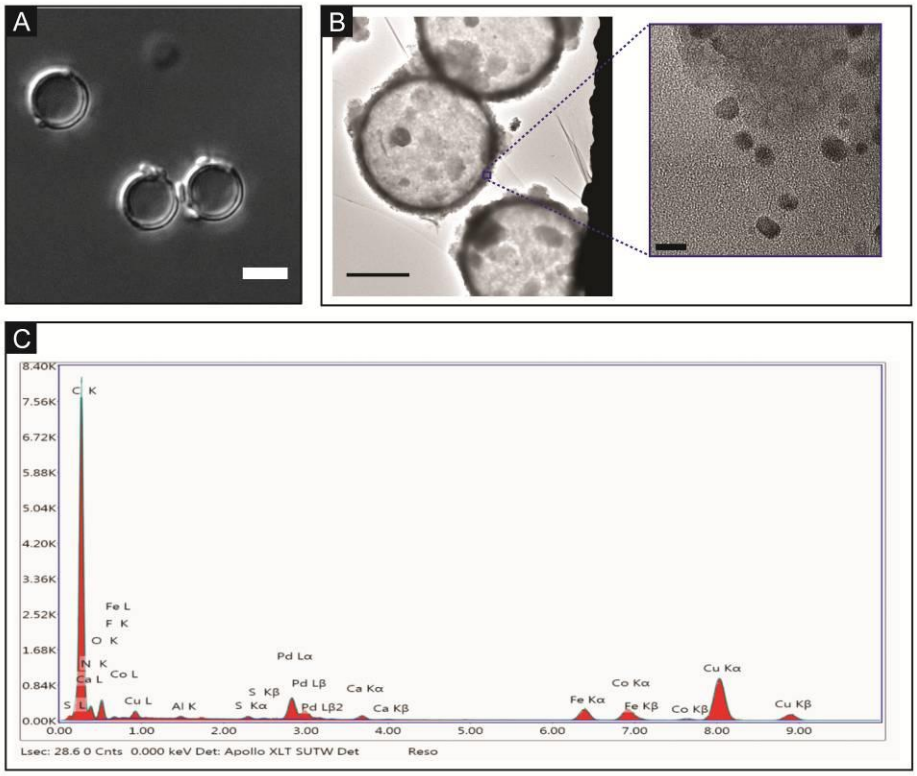

Figure S5. A) DIC micrograph of PVal-shells after *in situ* formation of Pd nanoparticles (scale bar is 5 µm). B) TEM micrographs of PVal-shells impregnated with Pd nanoparticles (scale bar is 2 µm, inset scale bar is 10 nm). C) STEM elemental analysis showing peaks corresponding to Pd nanoparticles.

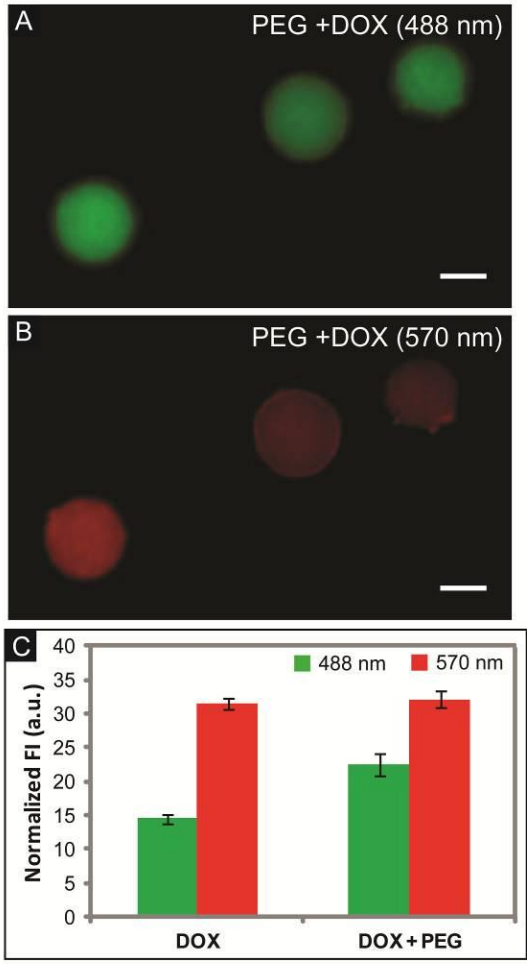

Figure S6. PVal negative-replica matrices fluoresces A) green at 488 nm and B) red at 570 nm after the entrapment of doxorubicin hydrochloride and PEG488. C) Increase in fluorescent intensity at 488 nm associated with the conjugation of PEG488.